Spectroelectrochemical Investigation of Double-Walled Tubular J-Aggregates of Amphiphilic Cyanine Dyes

ARTICLE *in* THE JOURNAL OF PHYSICAL CHEMISTRY C · JANUARY 2008

Impact Factor: 4.77 · DOI: 10.1021/jp077412f

6 AUTHORS, INCLUDING:

Stefan Kirstein
Humboldt-Universität zu Berlin
74 PUBLICATIONS **3,074** CITATIONS
SEE PROFILE

Jürgen P. Rabe
Humboldt-Universität zu Berlin
386 PUBLICATIONS **13,362** CITATIONS
SEE PROFILE

David Anton Vanden Bout
University of Texas at Austin
132 PUBLICATIONS **3,008** CITATIONS
SEE PROFILE

Spectroelectrochemical Investigation of Double-Walled Tubular J-Aggregates of Amphiphilic Cyanine Dyes

Jennifer L. Lyon,[†] Dörthe M. Eisele,[‡] Stefan Kirstein,[‡] Jürgen P. Rabe,[‡] David A. Vanden Bout,[†] and Keith J. Stevenson*[,†]

Department of Chemistry and Biochemistry, Center for Electrochemistry, The University of Texas at Austin, Austin, Texas 78712, and Department of Physics, Humboldt University, Newtonstr. 15, D-12489 Berlin, Germany

Received: September 14, 2007; In Final Form: October 29, 2007

The amphiphilic cyanine dye 3,3′-bis(2-sulfopropyl)-5,5′,6,6′-tetrachloro-1,1′-dioctylbenzimidacarbocyanine (C8S3) self-assembles in aqueous solution to form double-walled, tubular J-aggregates with ∼13 nm diameters and lengths up to several hundred nanometers. The redox and light absorption properties of immobilized J-aggregates on transparent, conductive indium tin oxide (ITO) electrodes have been studied directly using cyclic voltammetry (CV) in conjunction with UV−vis spectroscopy to elucidate unique mechanistic features of J-aggregate oxidation. Morphological properties were examined using in situ atomic force microscopy (AFM). Irreversible J-aggregate oxidation appears to occur primarily along the outer wall of the tubular structure as evidenced by the potential-induced irreversible bleaching of J-band absorption. Voltammetric studies as a function of scan rate and pH indicate that J-aggregate oxidation involves both electrochemical and chemical steps in which dimerization and subsequent dehydrogenation of the J-aggregate leads to the formation of a new dehydrogenated dimer oxidation product. This dehydrogenated dimer exhibits an absorbance band near 560 nm along with a reversible reduction peak characteristic of a surface-confined, redox-active species. Excellent correlation of J-aggregate redox potentials with spectroelectrochemical data is obtained that allows us to understand energetic thresholds for electron transfer in C8S3 tubular J-aggregates.

Introduction

Cyanine dyes have long been recognized as important spectral sensitizers for photographic imaging[1−9] and nonlinear optics[10,11] applications due to their extraordinarily sharp absorption bands arising from their large, highly delocalized π-conjugated systems and their aggregation properties. They are also well established as model systems for studies of photoactivated electron transport processes using monolayer assemblies at solid state[12,13] and liquid interfaces.[14]

When cyanine dyes are dispersed in polar solvents above a critical concentration level (usually low μM), they self-assemble into aggregates, known either as H- or J-aggregates depending on whether their excitonic absorption is blue- or red-shifted, respectively, relative to that of the dye monomer. Although the unique properties of cyanine dye J-aggregates, such as their highly efficient energy transfer properties, have been realized for decades,[15−18] most recently they have received attention for use in artificial light harvesting systems (LHS), since the J-aggregate architecture resembles that of naturally occurring LHS in photosynthetic bacteria.[19−22] Artificial LHS composed of J-aggregates that mimic natural LHS have been proposed, and their physicochemical properties have been explored in terms of their self-assembled structure and fast energy migration.[22,23] Unfortunately, the energy migration characteristics of self-assembled J-aggregate systems can vary widely based on aggregate morphology and spatial arrangement of dye molecules within the aggregates, which is controlled by the chemical structure and functional groups of the particular cyanine dye. In efforts to better correlate structure−property relationships in J-aggregate architectures, systematic studies correlating the optical properties and morphologies of 5,5′,6,6′-tetrachlorobenzimidacarbocyanine dye J-aggregates have been explored, focusing on the effects of functional group substitution at the 1,1′ and 3,3′ nitrogen positions on the resulting J-aggregates' morphologies. Dähne and Kirstein et al. have shown that creating an amphiphilic dye monomer through substitution of hydrophilic and hydrophobic groups at the 1,1′ and 3,3′ nitrogen positions results in an aggregation process driven by both van der Waals and hydrogen bonding forces, along with electrostatic repulsion due to delocalized charge along the chromophore backbone.[24−26] Importantly, the composition of the hydrophilic functional group has been shown to significantly affect the resulting J-aggregate morphology: if the solvent conditions are adjusted properly, a chromophore with carboxy-substituted 3,3′ nitrogen positions forms superhelical strands of double-walled tubules, whereas the same chromophore with sulfo-substituted 3,3′ nitrogen positions forms individual double-walled tubules.[27−30] This 3,3′ sulfo-substituted chromophore, based on the cyanine dye 5,5′,6,6′-tetrachlorobenzimidacarbocyanine and featuring hydrophobic octyl chains at the 1,1′ nitrogen positions, is abbreviated C8S3 and is shown in Scheme 1. The hydrophilic and hydrophobic regions of C8S3, when dispersed in a polar solvent such as water in the presence of 10 wt % methanol, align themselves in a bilayer-like structure in which the hydrophobic regions maintain minimal contact with water to form the double-walled, tubular J-aggregate structure represented pictorially in Scheme 1. The proposed double layer structure

* Corresponding author. E-mail: stevenson@cm.utexas.edu. Phone: (512) 232-9160. Fax: (512) 471-0985.
[†] The University of Texas at Austin.
[‡] Humboldt University.

10.1021/jp077412f CCC: $40.75
Published on Web 01/08/2008

SCHEME 1: (Left to Right) Chemical Structure of C8S3 Cyanine Dye, Showing the Most Hydrophilic and Hydrophobic Regions; Simple Sketch of Bilayer Formation (Not Scaled); Top View of Double-Walled Tubule Formed by the Bilayer (Not Scaled, Simplified); Three-Dimensional Image of Helical, Double-Walled Tubule

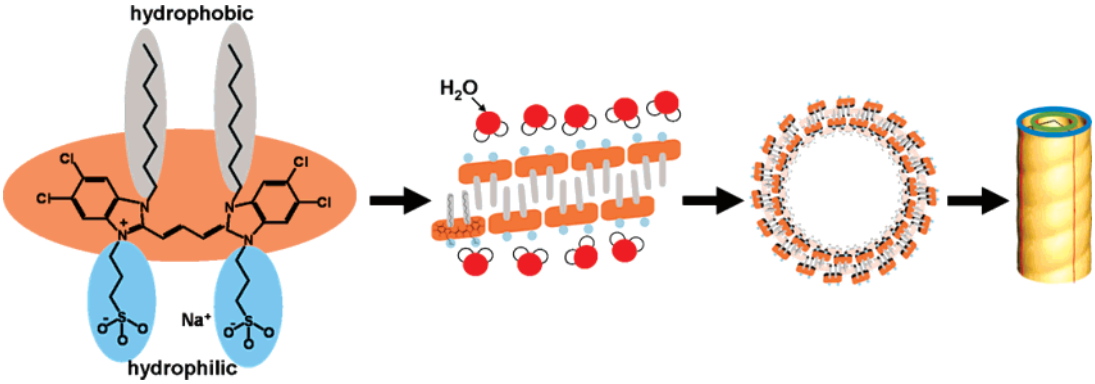

was confirmed by cryogenic transmission electron microscopy (TEM)[29] as well as by polarized absorption spectroscopy[28] and theoretical calculations.[31]

The double-walled tubular structure for C8S3 J-aggregates makes them extremely attractive for use in artificial LHS studies, due to its ordered, quasi-one-dimensional structure that allows investigation of energy migration and charge-transfer processes through observation of fluorescence quenching. Preliminary studies have indicated that solutions of noble metal salts (Ag and Pd) added to C8S3 J-aggregates result in the formation of metal nanoparticles along the outer wall of the tube.[32] It is assumed that electrons are transferred from the J-aggregate to reduce the metal salt; that is, the J-aggregate is oxidized at the expense of the nucleation and growth of metal nanoparticles. However, the resulting effect of J-aggregate oxidation in the presence of metals upon the aggregates' morphology remains unclear, as well as the exact mechanism of particle nucleation. Furthermore, the double-walled tubular morphology is destroyed upon decoration with Pd, yet it apparently remains intact when using Ag. Necessary fundamental information regarding the intrinsic redox and electron-transfer properties of the C8S3 J-aggregate system has not yet been elucidated. Herein we report spectroelectrochemical studies to examine the redox and absorption properties of immobilized J-aggregates on transparent, conductive indium tin oxide (ITO) electrodes. Cyclic voltammetry (CV) in conjunction with UV−vis spectroscopy is used to elucidate unique mechanistic features of C8S3 J-aggregate redox activity. This work builds upon the limited electrochemical studies of immobilized cyanine dye J-aggregates in aqueous solution,[33,34] as the majority of reports have concentrated solely on understanding the electrochemical behavior of cyanine dye monomers in organic solvents.[4−9] Excellent correlation of J-aggregate redox potentials with spectroelectrochemical data is obtained allowing us to associate observed optical phenomena with electron-transfer processes in the J-aggregates. J-aggregate oxidation is hypothesized to occur primarily along the outer wall of the double-walled structure, with no loss in long-range structure or morphology. The initial one-electron oxidation product of the J-aggregate is not stable and reacts in a chemical step to form a stable, dehydrogenated dimer oxidation product that exhibits its own unique redox and spectral activity.

Experimental Section

C8S3 J-Aggregate Preparation. The amphiphilic cyanine dye 3,3′-bis(2-sulfopropyl)-5,5′,6,6′-tetrachloro-1,1′-dioctylbenzimidacarbocyanine (C8S3) is available as a sodium salt from FEW Chemicals (Dye S 0440, FEW Chemicals, Germany) and was used as received. A 3.00 mM stock solution of monomeric C8S3 was prepared by dissolving an appropriate amount of C8S3 (MW = 902.8 g/mol) in pure methanol (Fisher Scientific) with stirring, forming a clear red solution. To prepare C8S3 J-aggregates, 130 μL of the C8S3 stock solution was added to 500 μL of ultrapure H_2O (>18.2 MΩ cm, Barnstead) and agitated to ensure even mixing. An immediate color change from clear red to opalescent, bright pink was observed, indicating the formation of double-walled tubular C8S3 aggregates.[29] The solution was stored in the dark for 24 h before adding an additional 500 μL of H_2O to stabilize the aggregation process, resulting in a final dye concentration of 3.36×10^{-4} M. Solutions of J-aggregates were typically used for experiments within 5 days of preparation and stored in the dark when not in use. Absorption measurements of C8S3 monomer and J-aggregate solutions were collected using an Agilent Instruments 8453 UV−visible spectrometer with a photodiode array detector. The measurement cell consisted of two quartz slides (0.1 mm path length) containing 45 μL of either monomer or J-aggregate solution.

Electrochemical Measurements. Electrochemical experiments were conducted on J-aggregates immobilized on transparent, conductive indium tin oxide (ITO)-coated glass electrodes (Delta Technologies, Ltd.; 14 Ω/□ immersed in an aqueous solution containing 1 M KNO_3 supporting electrolyte (Fisher Scientific). The pH of this supporting electrolyte was 5.78 ± 0.03 as prepared. For pH dependence studies, the pH of the KNO_3 solution was adjusted by adding small quantities of either 1 M HNO_3 or 1 M NaOH. Prior to use, the ITO working electrode substrates were cleaned by immersion in 30% (v/v) aqueous ethanolamine (Aldrich) at 80 °C for 20 min, followed by rinsing with methanol and sonicating in ultrapure H_2O for 30 min. The substrates were then dried under a stream of nitrogen. Films of J-aggregates were prepared on ITO by drop casting 10 μL of J-aggregate solution on a 0.5 cm^2 area of ITO followed by drying in the dark for ∼2 h. Once dried, they remained at the ITO surface when immersed in supporting electrolyte.

C8S3 monomer electrochemical experiments were conducted in 1.00 mM solutions of C8S3 in methanol containing 0.1 M tetrabutylammonium hexafluorophosphate supporting electrolyte (TBA-PF_6, Aldrich). Prior to its dissolution in methanol, the supporting electrolyte was recrystallized three times from absolute ethanol and dried under vacuum overnight. An ITO working electrode area of 0.5 cm^2 was immersed directly into the C8S3 solution.

ITO working electrodes, either bare or with dried J-aggregate films, were fitted in a 20 mL glass cell containing ∼5 mL

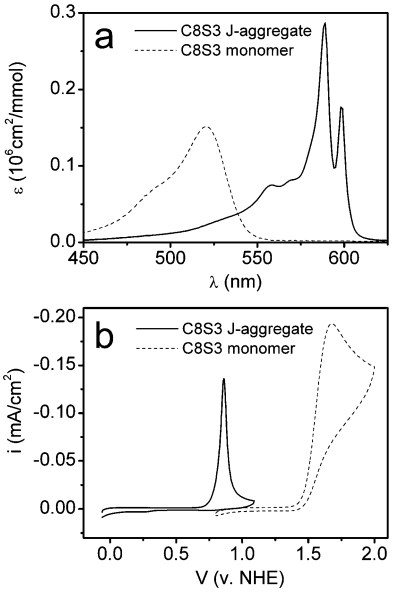

Figure 1. (a) C8S3 monomer (dashed line) and J-aggregate (solid line) absorbance spectra. (b) Cyclic voltammograms for 1 mM C8S3 monomer in methanol containing 0.1 M TBA-PF_6 at ITO (dashed line) and J-aggregates immobilized on ITO (solid line) in pH 5.78, 1 M KNO_3. Scan rate: 0.1 V/s.

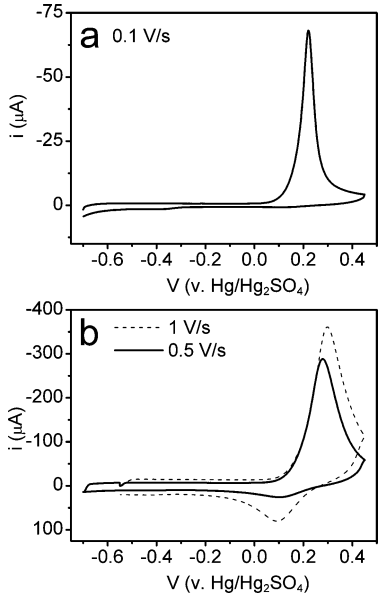

Figure 2. Cyclic voltammograms showing J-aggregate oxidation in pH 5.78, 1 M KNO_3 as a function of scan rate: (a) 0.1 V/s; (b) 0.5 V/s (solid line) and 1 V/s (dashed line).

supporting electrolyte and a Au wire counter electrode, with the ITO surface oriented perpendicular to the bottom of the cell. For aqueous measurements of J-aggregates, a Hg/Hg_2SO_4 (sat'd. K_2SO_4) reference electrode (CH Instruments; $E° = +0.640$ V vs NHE) was used. For C8S3 monomer measurements in methanol, a home-built Ag/AgO_x wire quasireference electrode ($E° = +0.799$ V vs NHE) was used, which was calibrated against the Fc/Fc^+ redox couple.[35] Electrochemical measurements were performed at room temperature (23 ± 2 °C) using an Autolab PGSTAT30 potentiostat interfaced with Autolab GPES version 4.9 software. Prior to each experiment, the cell was purged with Ar for at least 5 min. All experiments were conducted under flowing Ar unless otherwise noted. To compare electrochemical data between the aqueous and nonaqueous systems (Figure 1b, vida infra), electrode potentials were normalized to NHE. All other electrode potentials are reported vs Hg/Hg_2SO_4.

In Situ Atomic Force Microscopy Measurements. In situ AFM measurements were performed using a Digital Insturments MultiMode AFM with Nanoscope IIIa controller (Veeco Instruments, Santa Barbara, CA) operating in tapping mode with silicon nitride cantilevers (model DNP, Cr−Au backside coating, force constant = 0.12 N/m). All images were acquired at 0.3 Hz per line. A fluid cell containing pH 5.78, 1 M KNO_3 supporting electrolyte, a Pt wire counter electrode, and Ag/AgO wire quasi-reference electrode (QRE) calibrated against the Fc/Fc^+ redox couple was used.[35] A portion of the ITO working electrode, isolated from the J-aggregate film and supporting electrolyte, was electrically contacted using copper tape. The potential was controlled using a BAS CV-27 potentiostat (West Lafayette, IN). These experiments were performed in ambient air.

Spectroelectrochemical Measurements. Spectroelectrochemical experiments were performed using a CH700 bipotentiostat (CH Instruments) interfaced to an Agilent Instruments 8453 UV-Visible spectrometer with a photodiode array detector. A homemade electrochemical cell with a fixed working electrode area of 0.45 cm^2 and ~1 mL 1 M KNO_3 supporting electrolyte was placed in the spectrometer sample holder with the J-aggregate film-coated ITO working electrode in the beam path. The cell also contained a Pt wire counter electrode and Hg/Hg_2SO_4 (sat'd. K_2SO_4) reference electrode. The potential was cycled between −0.7 and +0.45 V for 3 consecutive cycles while absorption spectra between 350 and 800 nm were collected every 4.0 s with a 0.5 s integration time.

Results and Discussion

C8S3 dye molecules in aqueous solution form double-walled, tubular J-aggregates with lengths of several hundreds of nanometers and diameters of ~13 nm, with both the inner and outer wall possessing hydrophilic $-SO_3$ groups and the C8 chains protected from aqueous solution in the wall interior as documented previously.[29] The formation of J-aggregates is evidenced by the appearance of a characteristic red-shifted absorption spectrum relative to that of the C8S3 monomer, as shown in Figure 1a, with sharply defined J-aggregate absorbance maxima at 590 and 600 nm corresponding to the outer and inner wall tubular structure, respectively.[29,31] In addition to marked differences in the absorption spectrum, the redox properties of immobilized J-aggregates and C8S3 monomer also differ substantially. Figure 1b depicts cyclic voltammograms (CVs) showing the irreversible oxidation of both C8S3 monomer at ITO in 0.1 M methanolic TBA-PF_6 (dashed curve) and immobilized J-aggregates at ITO in aqueous pH 5.78, 1 M KNO_3 (solid line), both normalized to the NHE potential scale. The J-aggregates are significantly easier to oxidize, as reflected by a less positive potential of +0.861 V compared to that seen for the monomer at +1.675 V. These observations are consistent with those reported for other J-aggregate systems by Kawasaki et al., who showed that a lower oxidation potential is reflective of a lower activation energy for J-aggregate oxidation relative to cyanine monomers due to a shift in HOMO−LUMO energy levels upon aggregation.[33] Furthermore, spectroscopic studies probing the chemical oxidation of cyanine dyes adsorbed to AgBr microcrystals have found that the singlet excited-state energy of J-aggregates is much lower than that of its monomer.[8]

Figure 2 shows the voltammetric response for immobilized J-aggregates at ITO as a function of scan rate. At slow scan rates (<0.5 V/s), such as the 0.1 V/s scan shown in Figure 2a,

J-aggregate oxidation is irreversible, as evidenced by the lack of an appreciable reduction peak. Only a sharp oxidation peak is seen for the first anodic scan, with no corresponding reduction peak and no further oxidation apparent in subsequent voltammetric cycles. Other reports have observed that J-aggregate oxidation is irreversible for cyanine dye J-aggregates immobilized at modified Au (111).[33] Assuming a 1-electron process similar to electrochemical cyanine dye oxidation mechanisms reported previously,[4,5,9] integration of this peak indicates that ~0.56 nmol of dye has been oxidized, which corresponds to ~37% of the total amount of dye immobilized on the ITO working electrode. Because the J-aggregates are simply drop cast on the ITO surface without the use of a template or other methods to control their placement or alignment, the aggregates are randomly oriented in a film several layers thick (see in situ AFM data vida infra); it is thus conceivable that only a fraction of the J-aggregates are sufficiently close to the ITO surface to undergo direct electron transfer. Alternatively, Kawasaki et al. have suggested that repulsion of excessive delocalized positive charges along the dye molecules in the J-aggregate limits the extent of oxidation possible.[33] We note that replicate experiments of 10 trials show identical, reproducible behavior corresponding to irreversible J-aggregate oxidation centered at $+0.222 \pm 0.001$ V v. Hg/Hg_2SO_4 (+0.862 vs NHE) at 100 mV/s.

The irreversible oxidation of similar cyanine dye monomer and J-aggregates has been previously reported.[4,5,9,33] More specifically, Lenhard et al. have exhaustively studied the electrochemistry of more than two dozen cyanine dye monomers[4,5,9] and have concluded that the irreversible oxidation of the dye results from the formation of a dye radical dication which rapidly dimerizes with another dye molecule in solution to offset repulsive forces between them, preventing reduction of the oxidized dye radical dication. Such a scheme involves an electrochemical step followed by a chemical step, or "EC" mechanism

$$\mathrm{dye}^{+} \rightarrow \mathrm{dye}^{2+\bullet} + \mathrm{e}^{-} \quad (1)$$

$$2\mathrm{dye}^{2+\bullet} \rightarrow \mathrm{dimer}^{4+} \quad (2)$$

Furthermore, Lenhard et al. also established that a 2-proton, 2-electron loss following dimerization can occur, leading to the formation of an oxidized, dehydrogenated dimer (DHD_{ox})[4,5]

$$\mathrm{dimer}^{4+} \rightarrow \mathrm{DHD_{ox}}^{4+} + 2\mathrm{H}^{+} + 2\mathrm{e}^{-} \quad (3)$$

Although the mechanism schematics in Lenhard's work depict the 2-proton loss preceding the 2-electron loss in a separate step, it is noted that the $dimer^{4+}$ to DHD_{ox}^{4+} transition is often driven to occur at a potential very near that of J-aggregate oxidation.[5] Electrochemical studies of small chromophore dimerization mechanisms by others have also reported similar potential "compression", in which steric effects initiated by an initial electrochemical oxidation step alter molecular orbital energies, causing subsequent oxidation potentials to overlap, or in some cases even precede, that of the initial electron loss.[36−38] Therefore, though reaction (3) involves electron transfer, we may not observe a CV peak uniquely corresponding to this process; instead, the anodic peak at +0.222 V in Figure 2a may reflect both J-aggregate oxidation (1) and dimer oxidation to yield DHD_{ox}^{4+}(3). This means that the 37% efficiency of J-aggregate oxidation determined via integration of the anodic peak in Figure 2a may be an overestimate. Kawasaki has estimated that each dye molecule in immobilized thiacarbocyanine J-aggregates give up ~4e-/dye molecule when irreversibly oxidized at Au electrodes.[33] If $4e^{-}$/dye is the case, then only about 5% of the dye molecules in the C8S3 may be oxidized. Although it is not entirely clear whether both reactions (2) and (3), or only reaction (2), has occurred immediately following J-aggregate oxidation to prevent reduction of the radical dication, it has been demonstrated previously that reversible oxidation of the cyanine dye monomer may be achieved at sufficiently fast scan rates (200 V/s) so as to "outrun" the initial chemical step associated with the dimerization, reaction (2).[4] Although not explicitly attributed to kinetics of $dimer^{4+}$ or DHD_{ox}^{4+} formation, Kawasaki et al. have observed that oxidation of J-aggregates immobilized on cysteamine-modified Au electrodes is likewise irreversible at slower scan rates, yet becomes more reversible at faster (0.5−1 V/s) scan rates.[33] We also observe a similar scan rate dependence for scan rates >0.5 V/s, as shown in Figure 2b with the appearance of a cathodic peak at +0.093 V, corresponding to the reduction of a radical dication species that has not dimerized. However, the voltammograms presented in Figure 2 never approach true redox reversibility, suggesting that the 1 V scan rate is still not fast enough to outpace the chemical step for $dimer^{4+}$/ DHD_{ox}^{4+} formation. Unfortunately, we were unable to obtain data for scan rates >3 V/s due to excessive background charging currents at the ITO working electrode. To some extent, this is an expected result, as the close proximity of oxidized J-aggregate molecules in the J-aggregate structure should promote more facile $dimer^{4+}$/DHD_{ox}^{4+} formation than that seen for cyanine monomers in acetonitrile solvent. As such, Figure 2b supports the proposed mechanism of a 1-electron oxidation step followed by an irreversible chemical step associated with a dimerization reaction. Possibly a second chemical step involving further dehydrogenation to form DHD_{ox} occurs on a faster time scale that we are unable to resolve using our ITO working electrode. A previous report by Lenhard and Parton estimated that the irreversible dimerization of the radical dication occurs on a millisecond time scale, which is too fast to observe in our electrochemical experiments.[6]

We postulated that the dehydrogenation step associated with DHD_{ox} formation should also be reflected in voltammetric studies when conducted as a function of pH, in which J-aggregate oxidation should be more reversible at low pH, if reaction (3) is indeed contributing to the observed J-aggregate electrochemistry. Figure 3 shows a series of voltammograms in which immobilized J-aggregates on ITO were immersed in 1 M KNO_3 solutions of varying pH. To ensure that the immobilized J-aggregates' morphology was not compromised when immersed in more acidic and basic solutions, absorbance spectra were collected at each pH to verify the tubular structure (see the Supporting Information). From these spectra, we determined that immobilized J-aggregates at ITO immersed in 1 M KNO_3 solutions of pH 2.77−11.95 retained their tubular structure and could thus be compared directly. Figure 3a shows representative voltammograms acquired from immobilized J-aggregates at ITO immersed in 1 M KNO_3 solutions of pH 2.77−4.12, whereas Figure 3b shows the average ratio of the cathodic and anodic charge (Q_c/Q_a) obtained from integration of the cathodic and anodic peak currents estimated from three trials at all tested pH values. It can be seen from Figure 3 that the reversibility of J-aggregate oxidation is indeed dependent upon pH, with voltammograms conducted in more acidic pHs showing larger cathodic peak currents corresponding to the more facile reduction of the radical dication. At pH values >4.50, J-aggregate oxidation becomes completely irreversible, and the voltammograms take the shape of those featured in Figures 1b

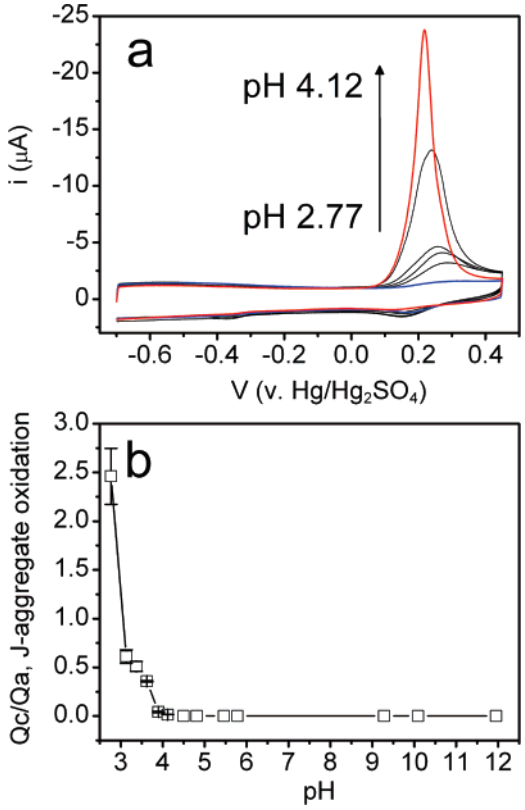

Figure 3. (a) Cyclic voltammograms of J-aggregate oxidation as a function of pH. Data only shown for pH values up to 4.12; see text for further discussion. (b) Ratio of integrated cathodic and anodic charge, Q_c/Q_a, for J-aggregate oxidation as a function of pH. Scan rate: 0.1 V/s.

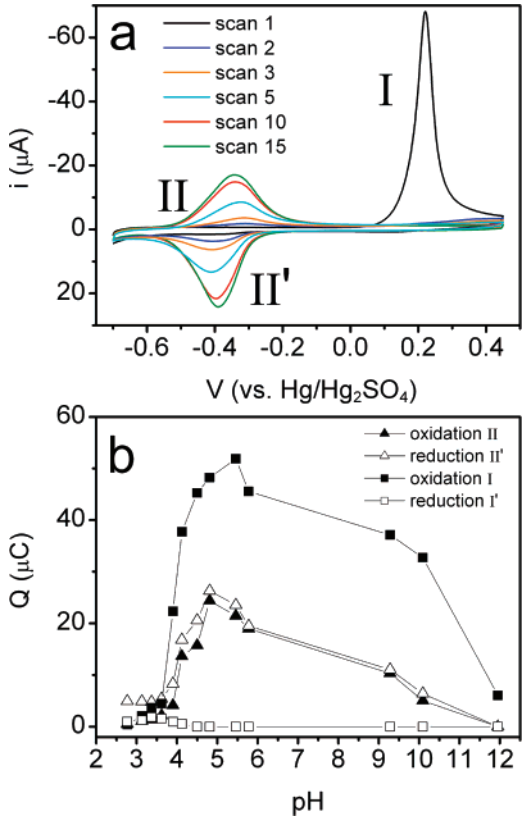

Figure 4. (a) Cyclic voltammograms displaying the formation of a second redox couple, II/II′, during potential cycling to induce J-aggregate oxidation (I) at an ITO electrodes in pH 5.78, 1 M KNO_3. (b) Integrated charge, Q, as a function of pH for the anodic current (filled triangles) and cathodic current (open triangles) for the redox couple II/II′ ($E_{1/2} = -0.378$ V), as well as the anodic (filled squares) and cathodic (open squares) charge corresponding to the redox couple I/I′ of J-aggregates.

and 2a. These results strongly suggest that a coupled proton-transfer reaction is involved with the chemical step(s) following the initial J-aggregate oxidation that ultimately prohibits the reduction of the radical dication and leads to the irreversible formation of the dimer product. Furthermore, these pH-dependent voltammetric studies suggest that the pK_a value for the C8S3 J-aggregate dimer lies between 4.12 and 4.50, since this pH range marks the transition between pseudo-reversible and irreversible oxidation behavior for the radical dication. Analysis of E_p values for pH 2.77−4.12 gives a slope of −27 mV/pH unit, which is close to the expected theoretical pH dependence on potential (59/n mV/pH unit, where n is the number of moles of electrons transferred) predicted for the 2-proton transfer proposed by Lenhard;[4,5] however, we also note that the shape of the J-aggregate oxidation peak transitions from a broad, wide peak to an extremely narrow peak with increasing pH, which may affect the apparent peak position. As shown in the integrated charge plot vs pH in Figure 3b, we note that J-aggregate oxidation remained totally irreversible at pH values above 4.50, though a gradual broadening of the anodic peak was again observed as the pH changed from neutral to basic (see the Supporting Information).

Lenhard et al. have also documented that reversible redox behavior for the DHD product formed from dimer dehydrogenation can be seen[4]

$$DHD_{ox}^{4+} + 2e^- \leftrightarrow DHD_{red}^{2+} \quad (4)$$

The formation and stability of the DHD species is strongly dependent upon the stability of the dye radical dication and its susceptibility to dehydrogenation.[4] Because the C8S3 J-aggregate exhibits such a strong susceptibility for dimer formation and subsequent dehydrogenation at neutral pH (cf. discussion of Figures 2 and 3), we expect to observe a reversible redox response for the DHD product in our voltammograms. Figure 4a shows a series of voltammograms collected for immobilized J-aggregates on ITO in pH 5.78, 1 M KNO_3 over a large potential window. As discussed above, the irreversible J-aggregate oxidation (labeled I, black trace) is seen at +0.222 V, but a second, reversible redox couple appears centered at $E_{1/2} = -0.378$ V, labeled II/II′. Note that the current response for this new reduction/oxidation process continues to increase until a steady-state response is obtained after ∼15 consecutive cycles. We propose that the new redox-active species (II/II′) is the DHD_{ox}^{4+} product resulting from the initial J-aggregate oxidation followed by dimerization and dehydrogenation steps. Further evidence supporting this hypothesis is shown in Figure 4b, in which the steady state integrated current of II/II′ is plotted as a function of supporting electrolyte pH, along with the integrated current associated with the J-aggregate redox couple (I/I′). From the figure, it is clearly evident that processes I and II/II′ follow the same pH dependence; that is, as a greater amount of J-aggregates are oxidized, a greater amount of II/II′ appears. All three redox processes (J-aggregate oxidation I, oxidation II ,and reduction II′) pass through a maximum near pH 5−6. Additionally, we note that voltammetric studies were conducted in which the potential window was varied for the immobilized J-aggregate ITO electrode and cycled 15 times without inducing J-aggregate oxidation (i.e., from the same negative extreme as that shown in Figure 4a to +0.025 V, just before the onset of J-aggregate oxidation; see the Supporting

SCHEME 2: Depiction of the Overall ECE Mechanism for C8S3 J-Aggregate Oxidation and Subsequent Dehydrogenated Dimer (DHD) Formation

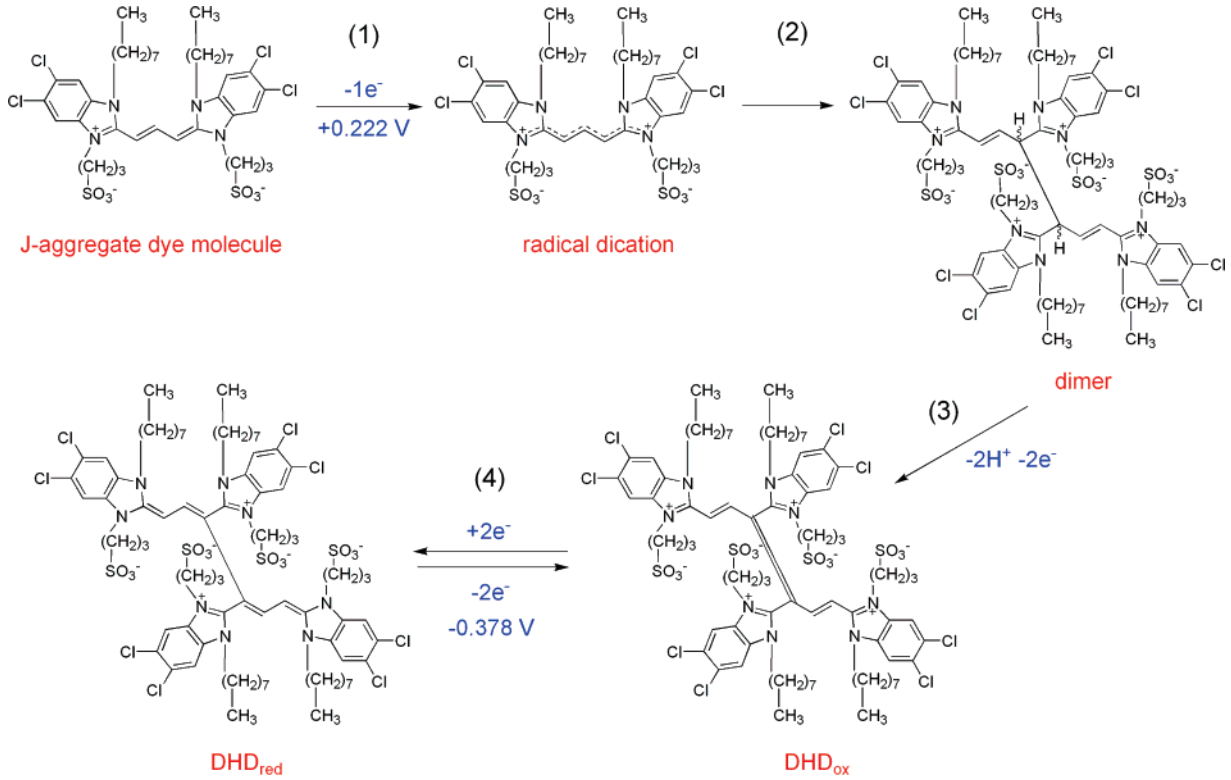

Information). In this case, we do not see the appearance of the redox response for II/II′. However, if the potential is then scanned positive (anodically) to +0.45 V to induce J-aggregate oxidation and form radical dications, the reduction peak II′ appears on the return sweep. From this data, it appears that II/II′ is indeed related to the J-aggregate oxidation process and is most likely reflective of a J-aggregate oxidation product whose redox activity behaves in accordance with Lenhard's proposed DHD redox mechanism, (4). Scheme 2 depicts our proposed potential-dependent mechanism of C8S3 J-aggregate oxidation and subsequent DHD_{ox}^{4+} formation in an electrochemical-chemical-electrochemical step (ECE) process that would require a net $4e^-$/dye molecule to yield the DHD_{ox}^{4+} product.

Though the DHD_{ox}^{4+} formation mechanism is derived from studies of cyanine dye monomers, it may be even more plausible in the case of J-aggregates, in which monomer units of dye are spatially arranged in close proximity to one another, promoting dimer associations of oxidized dye and the subsequent formation of DHD_{ox}^{4+}. If the species responsible for II/II′ in Figure 4a is a DHD_{ox}^{4+} product formed from neighboring dye molecules in the immobilized J-aggregates at ITO, then its voltammetric behavior should follow that predicted for a surface-confined redox species. We observe that peak currents for both II and II′ at steady-state scale linearly with increasing scan rate between 0.01 and 3 V/s, as predicted for a diffusionless system (see the Supporting Information). Additionally, the peak-to-peak separation (ΔE_p) of II/II′ may be analyzed to determine an apparent electron-transfer rate constant (k_{obs}^0) as predicted by Laviron's model for surface-confined redox species,[39] with ΔE_p at the slowest scan rates approaching 0 V, the theoretical value for an adsorbed redox couple.[40] From the experimental ΔE_p values, k_{obs}^0 was estimated at 5.3 s^{-1}. Similar values of k_{obs}^0 have been observed when studying other macromolecular, surface-confined systems such as protein films at ITO.[41] To further probe whether the proposed J-aggregate oxidation product, DHD_{ox}^{4+}, is surface-confined, we conducted in situ AFM experiments to investigate any changes in J-aggregate film topography prior to, during and after electrochemical oxidation. Figure 5 shows in situ AFM images of immobilized J-aggregates at ITO immersed in pH 5.78, 1 M KNO_3 collected at open circuit (pre-oxidation, Figure 5a) and with an applied oxidative potential of +0.6 V vs Fc/Fc^+ (post-oxidation, Figure 5b). Cross-sectional height profiles for each of the images, measured for the regions denoted on the AFM images, are plotted in Figure 5c. From this data, it is evident that the oxidation of the J-aggregate film does not substantially alter the J-aggregates' long-range structure and morphology, as the difference in both height and topography between the two images is minimal. The AFM images indicate that the J-aggregates are randomly oriented within the film, as expected for a drop-cast film without templates or other directed assembly, while the height profile suggests the aggregates are stacked in layers of 1−4 aggregates, assuming a 13 nm J-aggregate diameter.[29] Given the relatively slow k_{obs}^0 value determined above along with the Faradaic current calculations from Figure 2a suggesting incomplete oxidation of the film, it is plausible that the topmost layers and outer wall components of the tubular J-aggregates, i.e., the ones which are mapped by the AFM tip, are relatively unaffected by the applied potential, leading to the observed similarities between the pre- and post-oxidation images in Figure 5. Even if this is the case, the oxidation of those J-aggregates on the outer wall closest to the ITO surface still does not appear to cause enough structural disruption to produce a change in morphology, again suggesting that the DHD_{ox}^{4+} product remains confined at the ITO surface.

To correlate the electrochemical oxidation of C8S3 J-aggregates with their well-defined absorption spectrum, spectroelectrochemical experiments were carried out in which the potential of an ITO working electrode containing a J-aggregate film was scanned concurrently with the acquisition of absorbance spectra in the visible region from 350 to 800 nm. Similar

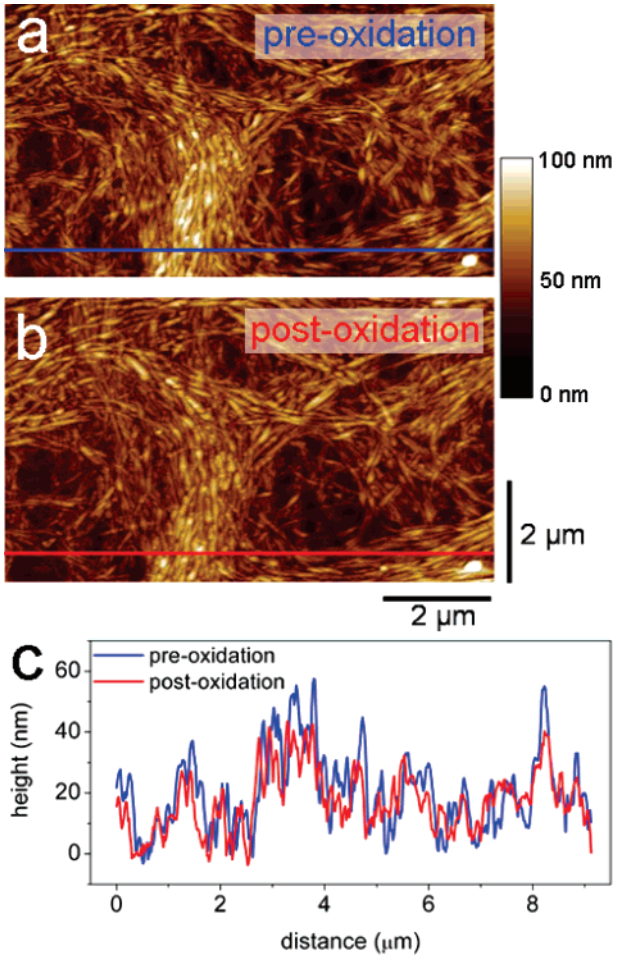

Figure 5. In situ AFM images of immobilized C8S3 J-aggregates on ITO immersed in pH 5.78, 1 M KNO_3 taken at (a) open circuit (−0.15 V vs Fc/Fc^+) and (b) at an oxidizing potential (+0.60 V vs Fc/Fc^+). (c) Cross-sectional height profiles of the regions defined in (a) and (b) by blue and red lines, respectively.

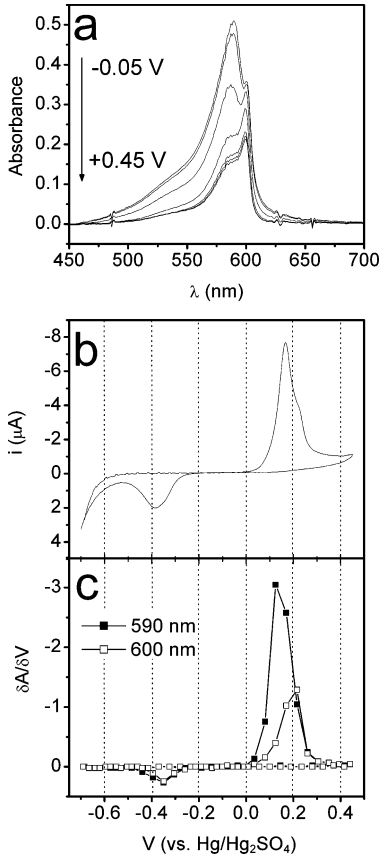

Figure 6. Spectroelectrochemical data for the oxidation of immobilized C8S3 J-aggregates on ITO: (a) absorption spectra versus applied potential, (b) cyclic voltammogram at 0.01 V/s in pH 5.78, 1 M KNO_3, (c) differential absorbance ($\delta A/\delta V$) plot for outer wall and inner wall J-aggregate absorbance bands centered at 590 and 600 nm, respectively.

studies have been undertaken previously to investigate J-aggregates organized on modified Au(111).[34] In order to maximize the number of spectra acquired for correlation to the CV, a slow scan rate of 0.01 V/s was used, permitting spectral acquisition every 45 mV. The results of this experiment are shown in Figure 6. Figure 6a depicts the decrease in absorbance observed upon electrochemical oxidation of the J-aggregate film. As more anodic potentials are applied, the absorbance at 590 nm corresponding to the outer wall of the J-aggregate tubular structure decreases dramatically. The inner wall absorbance at 600 nm also decreases, though not as substantially as that of the outer wall; the relative intensity of the inner wall in fact surpasses that of the outer wall as a result of electrochemical oxidation. This change in relative absorbance most likely reflects a more facile oxidation of the outer wall, due to outer wall dye molecules being in closer electrical contact with the electrode, along with a more hindered oxidation of the inner wall dye molecules due to their occlusion by the C8 chains, and a possible charge compensation hindrance due to slower ion transport within the interior of the tube. The integrated charge of the J-aggregate oxidation peak at +0.166 V in Figure 6b corresponds to 0.34 nmol, or ∼44% of the total amount of spectroscopically active J-aggregates present, as determined from the first acquired spectrum. [Because of the geometry of the cell used to acquire spectroelectrochemical data, some of the immobilized J-aggregates were contained outside the illumination window, resulting in a lower initial absorbance reading than that obtained for ITO slides with drop-cast J-aggregates not enclosed in the spectroelectrochemical cell. Therefore, the calculated relative percentage of electroactive J-aggregates in Figure 5 is higher than that in Figure 2 (50% vs 37%), even though the data in Figure 5 corresponds to fewer moles of electroactive J-aggregates (0.34 vs 0.56 nmol).] Accordingly, the peak intensity at 590 nm in Figure 6a has decreased by ∼50% during the course of the oxidation. Given that only half of the J-aggregates within in the film are oxidized, this result further supports the aforementioned discussion concerning slow interfacial electron transfer, particularly between inner wall dye molecules and the working electrode. Importantly, the absorption maxima do not shift as a function of applied potential, but rather remain fixed at 590 and 600 nm, respectively. Previous spectroscopic studies by Lenhard and Hein correlated wavelength shifts with disruption of the J-aggregate dye upon chemical oxidation;[8] in contrast, our results indicate again that the J-aggregates' morphology is not disturbed as a result of electrochemical oxidation, in agreement with the electrochemical AFM results.

As shown in Figure 6c, the differential absorbance ($\delta A/\delta V$) plots for both inner and outer wall oxidation correlate well with the voltammetric response in Figure 6b. Clearly, the $\delta A/\delta V$ plots nearly perfectly overlay the CV data, showing the direct correlation between electrochemical oxidation of the J-aggregates and changes in the J-band absorbance. At this slower scan rate, the J-aggregate oxidation peak in Figure 6b features a shoulder near +0.230 V in addition to the sharp oxidation at +0.166 V.

Closer inspection of Figure 6c reveals that the inner wall of the J-aggregate structure passes through a maximum in differential absorbance ~70 mV after the outer wall does and that the resulting differential absorbance plot very closely resembles the shouldered peak in Figure 6b. This observed lag between outer and inner wall oxidation further supports the aforementioned explanation of the change in their relative absorbance intensities. A subsequent cathodic potential sweep from +0.45 to 0 V (Figure 6b,c) shows neither J-aggregate electrochemical reduction nor an increase in J-band absorbance (inner or outer wall), agreeing with our electrochemical studies demonstrating the irreversibility of J-aggregate oxidation at neutral pH. This irreversible electrochemical process (reaction (1)) corresponds to irreversible J-aggregate bleaching, as evidenced by the unchanging differential absorbance observed at both 590 and 600 nm between +0.45 and 0 V in the cathodic sweep of Figure 6c.

On the return sweep of the voltammogram shown in Figure 6b, the reduction peak II′, corresponding to the reduction of DHD_{ox}^{4+} occurs at −0.378 V, and a response in the $\delta A/\delta V$ plots is observed concurrently. Assuming that only the absorbance bands centered at 590 and 600 nm are present in spectra during the course of this experiment, this data suggests that the J-band absorbance is increasing as DHD_{ox}^{4+} is reduced. However, examination of the full absorption spectrum reveals a new broad absorption generated upon reduction of II′ that overlaps with the aggregate peaks. This absorption correlates to the formation of DHD_{red}^{2+}. Subtraction of a spectrum taken immediately following reduction II′ from one immediately preceding reduction II′ yields the DHD_{red}^{2+}absorption spectrum (see the Supporting Information). Previous studies of cyanine dyes have shown that the DHD_{red}^{2+} spectrum generally resembles that of the monomer, while the DHD_{ox}^{4+} species is significantly blue-shifted.[5] These previously reported observations agree with our present observation that the product of the J-aggregate oxidation and dimer hydrogenation, DHD_{ox}^{4+}, is absent from our spectra. On the basis of both our results and the previously reported results, we believe that DHD_{ox}^{4+} is likely in the ultraviolet region (and thus not observed in our spectra) and that the species observed at 560 nm is DHD_{red}^{2+}. One would expect DHD_{red}^{2+} to be slightly blue-shifted from the monomer absorption, but our results yield a spectrum that is slightly red-shifted. This is likely due to the fact that in our case DHD_{red}^{2+} is confined to the aggregate structure, whereas previous studies have all examined dyes that are fully solvated.[5]

Conclusion

We have presented herein the first reported spectroelectrochemical studies of C8S3 cyanine dye double-walled tubular J-aggregates immobilized at an unmodified ITO electrode surface. The J-aggregates' irreversible redox behavior is similar to that observed in previous electrochemical studies of both solution-phase J-aggregates and cyanine dye monomers. The reversibility of J-aggregate oxidation depends strongly upon scan rate and pH, suggesting that both electrochemical and chemical steps are occurring in an overall ECE mechanism. In particular, both irreversible dimerization and dehydrogenation chemical steps appear to follow the initial oxidation, which leads to the formation of a dehydrogenated dimer oxidation product. This dehydrogenated dimer product exhibits its own unique redox activity and is most likely surface-confined, as indicated by both electrochemical analysis and in situ AFM measurements. Spectroelectrochemical studies show that the J-aggregate oxidation is mostly confined to the outer wall of the tubular structure and that the inner wall is oxidized to a lesser extent relative to the outer wall. These studies are fundamental to the understanding of photo- and electron-transfer processes in such cyanine dye J-aggregate systems. Elucidation of their physicochemical properties will facilitate their advanced application as enhanced spectral sensitizers for artificial light-harvesting systems.

Acknowledgment. Financial support for this work was provided by the R.A. Welch Foundation (Grant F-1529), the National Science Foundation (CHE-0134884), and Deutsche Forschungsgemeinschaft [Sfb 448: Mesoscopically Organized Composites]. We thank Ryan Williams for his assistance with the in situ AFM measurements.

Supporting Information Available: Absorbance spectra of J-aggregate films in 1 M KNO_3 solutions of varying pH, representative voltammograms of J-aggregates in neutral and basic pH solutions, voltammograms showing the absence of DHD_{ox}^{4+}/ DHD_{red}^{2+} redox activity in the absence of J-aggregate oxidation, scan rate dependence plots for determining k_{obs}^{0}, and subtracted UV−vis spectra depicting absorbance of DHD_{red}^{2+}. This material is available free of charge via the Internet at http://pubs.acs.org.

References and Notes

(1) West, W.; Gilman, P. B. In *The Theory of the Photographic Process*; James, T. H., Ed.; Macmillan: New York, 1977; pp 277.
(2) Mishra, A.; Behera, R. K.; Behera, P. K.; Mishra, B. K.; Behera, G. B. *Chem. Rev.* **2000**, *100*, 1973−2011.
(3) Shapiro, B. I. *Russ. Chem. Rev.* **2006**, *75*, 433−456.
(4) Lenhard, J. R.; Cameron, A. D. *J. Phys. Chem.* **1993**, *97*, 4916−4925.
(5) Parton, R. L.; Lenhard, J. R. *J. Org. Chem.* **1990**, *55*, 49−57.
(6) Lenhard, J. R.; Hein, B. R.; Muenter, A. A. *J. Phys. Chem.* **1993**, *97*, 8269−8280.
(7) Lenhard, J. *J. Imag. Sci.* **1986**, *30*, 27−35.
(8) Lenhard, J. R.; Hein, B. R. *J. Phys. Chem.* **1996**, *100*, 17287−17296.
(9) Lenhard, J. R.; Parton, R. L. *J. Am. Chem. Soc.* **1987**, *109*, 5808−5813.
(10) Kobayashi, T. In *J-Aggregates*; World Scientific: Singapore, 1996.
(11) Würthner, F.; Wortmann, R.; Meerholz, K. *ChemPhysChem* **2002**, *3*, 17−31.
(12) Dähne, S. *Photogr. Sci. Eng.* **1979**, *23*, 219−239.
(13) Tani, T.; Suzumoto, T.; Ohzeki, K. *J. Phys. Chem.* **1990**, *94*, 1298−1301.
(14) Kuhn, H.; Möbius, D.; Bucher, H. In *Physical Methods of Chemistry*; Weissberger, A., Rossiter, B. W., Eds.; Wiley: New York, 1972; Vol. I, Part IIB.
(15) Jelley, E. E. *Nature* **1936**, *138*, 1009.
(16) Jelley, E. E. *Nautre* **1937**, *139*, 631.
(17) Scheibe, G. *Angew. Chem.* **1936**, *49*, 536.
(18) Scheibe, G. *Angew. Chem.* **1937**, *50*, 212−219.
(19) Deisenhofer, J.; Michel, H. *Angew. Chem.* **1989**, *101*, 872−892.
(20) Huber, R. *Angew. Chem.* **1989**, *101*, 849−871.
(21) Koepke, J.; Hu, X. C.; Muenke, C.; Schulten, K.; Michel, H. *Structure* **1996**, *4*, 581−597.
(22) McDermott, G.; Prince, S. M.; Freer, A. A.; Hawthornthwaite-Lawless, A. M.; Papiz, M. Z.; Cogdell, R. J.; Isaacs, N. W. *Nature* **1995**, *374*, 517−521.
(23) Amerongen, H. v.; Valkunas, L.; Grondelle, R. v. In *Photosynthetic Excitons*; World Scientific: Singapore, 2000.
(24) Pawlik, A.; Ouart, A.; Kirstein, S.; Abraham, H.-W.; Dähne, S. *Eur. J. Org. Chem.* **2003**, *16*, 3065−3080.
(25) von Berlepsch, H.; Böttcher, C.; Ouart, A.; Burger, C.; Dähne, S.; Kirstein, S. *J. Phys. Chem. B* **2000**, *104*, 5255−5262.
(26) Pawlik, A.; Kirstein, S.; De Rossi, U.; Dähne, S. *J. Phys. Chem. B* **1997**, *101*, 5646−5651.
(27) Spitz, C.; Dähne, S. *Phys. Chem. Chem. Phys. Lett.* **1998**, *102*, 738−744.
(28) Pugzlys, A.; Hania, P. R.; Augulis, R.; Duppen, K.; Loosdrecht, P. H. M. v. *Int. J. Photoener.* **2006**, *2006*, 1−9.
(29) von Berlepsch, H.; Kirstein, S.; Hania, R.; Pugzlys, A.; Böttcher, C. *J. Phys. Chem. B* **2007**, *111*, 1701−1711.
(30) Kirstein, S.; Dähne, S. *Int. J. Photoener.* **2006**, *2006 (20363)*, 1−21.

(31) Didraga, C.; Pugzlys, A.; Hania, P. R.; von Berlepsch, H.; Duppen, K.; Knoester, J. *J. Phys. Chem. B* **2004**, *108*, 14976−14985.
(32) Kirstein, S.; von Berlepsch, H.; Böttcher, C. *Int. J. Photoener.* **2006**, *2006 (47917)*, 1−7.
(33) Kawasaki, M.; Sato, T. *J. Phys. Chem. B* **2001**, *105*, 796−803.
(34) Kawasaki, M.; Yoshidome, D.; Sato, T.; Iwasaki, M. *J. Electroanal. Chem.* **2003**, *543*, 1−11.
(35) Singh, P. S.; Evans, D. H. *J. Phys. Chem. B* **2006**, *110*, 637−644.
(36) Macias-Ruvalcaba, N. A.; Evans, D. H. *J. Phys. Chem. C* **2007**, *111*, 5805−5811.
(37) Levillain, E.; Roncali, J. *J. Am. Chem. Soc.* **1999**, *121*, 8760−8765.
(38) Raimundo, J.-M.; Levillain, E.; Gallego-Planas, N.; Roncali, J. *Electrochem. Commun.* **2000**, *2*, 211−215.
(39) Laviron, E. *J. Electroanal. Chem.* **1979**, *101*, 19−28.
(40) Bard, A. J.; Faulkner, L. R. In *Electrochemical Methods: Fundamentals and Applications*, 2nd ed.; John Wiley & Sons: Hoboken, NJ, 2001.
(41) El, Kasmi, A.; Leopold, M. C.; Galligan, R.; Robertson, R. T.; Saavedra, S. S.; El, Kacemi, K.; Bowden, E. F. *Electrochem. Commun.* **2002**, *4*, 177−181.